N85-22486

THREE-DIMENSIONAL CALCULATION OF SHUTTLE CHARGING IN POLAR ORBIT*

D. L. Cooke, I. Katz, M. J. Mandell, J. R. Lilley, Jr.
S-CUBED
La Jolla, California 92038

A. J. Rubin
Air Force Geophysics Laboratory
Hanscom Air Force Base, Massachusetts 01731

The charged particle environment in polar orbit can be of sufficient intensity to cause spacecraft charging. In order to gain a quantatative understanding of such effects, the Air Force is developing POLAR, a computer code which simulates in three dimensions the electrical interaction of large space vehicles with the polar ionospheric plasma. It models the physical processes of wake generation, ambient ion collection, precipitating auroral electron fluxes, and surface interactions, including secondary electron generation and backscattering, which lead to vehicle charging. These processes may be followed dynamically on a subsecond timescale so that the rapid passage through intense auroral arcs can be simulated. POLAR models the ambient plasma as isotropic Maxwellian electrons and ions (O^+, H^+), and allows for simultaneous precipitation of power-law, energetic Maxwellian, and accelerated Gaussian distributions of electrons. Magnetic field effects will be modeled in POLAR but are currently ignored.

The theoretical models and approximations employed in POLAR are discussed, including an effective process for stabilizing the Poisson-Vlasov iteration process in the short Debye length extreme. A preliminary POLAR calculation is presented which predicts the effects of measured auroral fluxes on the shuttle orbiter, and demonstrates the combination of conditions required for substantial differential charging of the orbiter.

INTRODUCTION

The charging of the space shuttle orbiter in the polar (auroral) ionosphere has been investigated by Katz and Parks (ref. 1). In that paper, the authors argue that observed precipitating electron fluxes can exceed the ram ion flux (~120 $\mu A/m^2$ for $n = 10^5$ cm^{-3}, $V = 8$ km/sec). This implies a possible overall current balance at a negative potential to enhance ion collection and retard electron fluxes. Both theoretical and experimental (refs. 2, 3, 4) studies have shown that as object dimensions become large with respect to the local Debye length, space charge effects will severely reduce the ion current collection compared to orbit limited theory. This leads to a "size-effect" for the potential buildup on objects subjected to auroral electron fluxes. Katz and Parks (ref. 1) have calculated, for a conducting

sphere, the equilibrium potential as a function of K, the ratio of secondary electron corrected precipitating electron flux to the secondary corrected ram ion flux. For a beam energy of 5 KeV and $K \approx 3$, a sphere radius to Debye length ratio of 10 leads to a potential of -100 volts, whereas a size ratio of 100 leads to a potential of -1300 volts.

The space shuttle is many times larger than any vehicle that has been previously flown through auroral regions. Consequently, the predicted size-effect on vehicle charging suggests that past experience will not be adequate for predicting and understanding the interactions of large objects with the auroral ionosphere.

An understanding of the charging dynamics of a real spacecraft requires more than a good probe theory. Differential charging depends on the often complex interplay of differing materials and their spatial relationships. The sunlight charging of ATS-6 (ref. 5) provides an example of how a charging surface can create electrostatic barriers that will bootstrap the entire vehicle to a highly charged state.

Thus, for a little more than a year, S-CUBED has been developing the computer code, POLAR, with the following design criteria:

- Three-dimensional
- Quasistatic
- Flexible plasma parameters including flow
- Magnetic field effects
- Complex geometries, electrical model
- Material effects
- Wake model
- Self-consistent inclusion of space charge effects
- Small (core storage)
- Fast

The preliminary version of POLAR is nearly complete. This paper will outline physical models and computational techniques, review the current program status, and present preliminary calculations of auroral charging.

POLAR

Why a three-dimensional code? Results from a 3-D code can be compared directly to satellite data during validation without the interpretational uncertainties that spring from reduced dimensional models. This benefit will ultimately carry over as POLAR becomes a design tool for structures with limited symmetry. Also, arbitrary arrangements of vehicle velocity, magnetic field, sun angle, and vehicle orientation, can only be properly modeled in three-dimensions. It can be argued that solving problems in 3-D within reasonable machine limits can compromise the accuracy of the physics, and/or result in an impractical program. With this in mind, the POLAR design philosophy dictates the limited use of particle tracking methods in favor of coordinated approximations and analytic models.

POLAR is a quasistatic code. That is, it employs implicit timestepping to follow surface charging where timescales, τ, are determined by incident currents and vehicle capacitances (10^{-3} sec $< \tau < 10^2$ sec), but assumes that the plasma environment is always in steady state. In the future, we may find

it necessary to include wave effects and turbulent phenomena by the use of time averaged models, diffusion rates, heating, etc.

The lower auroral ionospheric environment is summarized in Table 1. The values given in the table are considered typical, but none are fixed in POLAR where these and other parameters (such as the oxygen to hydrogen ion ratio) are variable over wide ranges. The energetic electron spectrum is currently modeled as a sum of power law, hot Maxwellian, and Gaussian distributions.

POLAR presently ignores the magnetic field; however, its inclusion is a current effort. Some of the methods under study for including magnetic effects are:

Place $\vec{v} \times \vec{B}$ potential gradient on the vehicle.
Include $\vec{B}$ in ion trajectories interior to sheaths.
Pitch angle conics for the energetic electrons (presently, isotropy is assumed).
Modification of secondary and photoelectron emission where $\vec{B}$ parallels a surface.
Modification of secondary and photoelectron surface conductivities in directions perpendicular to $\vec{B}$.

We now outline the methods used in POLAR to perform charging calculations. A calculation is broken in to the major steps listed below:

Vehicle definition.
Environment specification and computational grid construction.
Presheath and wake ion density calculation.
Initial surface charging using flux estimates.
* Poisson and electron charge density calculation.
* Sheath determination and particle (ions) tracking to determine:
      sheath ion densities
      ion surface currents
* Surface charging.

After all of the above modules have been executed once, the * items are iterated upon to produce a final solution. At this stage in the development of POLAR, only negative surface potentials are allowed. Although slightly positive potentials could occur under natural charging conditions due to secondary or photoelectron emission, the ambient electrons should limit positive potentials to a few kT at most. With this constraint, electrons are considered to be repelled with densities given by the Boltzmann expression, $n_e = n_0 \exp(-qV/kT)$. The methods used to calculate the attracted ion densities are described later in this paper.

Positive potentials may also be achieved by the emission of electrons (ref. 6). The physics of electron collection in the lower ionosphere appears more complex than the collection of ions due to turbulent processes in both the emitted beams and in the ambient plasma (refs. 7, 8). Thus, spacecraft generated high positive potentials are not now considered in POLAR but will be addressed in future work.

OBJECT DEFINITION

POLAR objects are built from the same set of blocks used in NASCAP (ref. 9) with the addition of slanted thin plates and the exclusion of booms. These blocks are illustrated in figure 1. These blocks can be easily combined to construct complex objects as illustrated by our model of the shuttle orbiter, shown in figure 2. Objects are defined on a variably sized object grid of cubic volume elements. Since POLAR must model objects moving at high ion Mach numbers, the extended ion wake is included in the computation by embedding the object space in a sliced, staggered computational grid. Figure 3 illustrates the arrangement of object, object grid, Mach vector, and computational grid. All data arrays are sliced into individual NX*NY pages at every Z mesh point, and stored on disk. During computation, POLAR will page into core only the required set of slices. Using the potential array as an example, the Poisson solver will need only two slices at a time; the sheath location algorithm, four slices; and the trajectory tracker, two slices.

Since the data structure is sliced along the $\hat{Z}$ axis, the Mach vector is constrained to have a dominant $\hat{Z}$ component. When other arrangements of Mach vector and object orientation are to be modeled, POLAR can rotate the object and Mach vector to meet this constraint, thus avoiding a redefinition of the object.

PRESHEATH AND WAKE ION DENSITIES

POLAR utilizes a sharp edged sheath approximation to divide space into presheath and sheath regions. The sheath region contains all of the significant space charge, while the presheath is a quasineutral region. The wake region is divided by the sheath edge, with the extended wake assumed to be essentially quasineutral and included with the presheath. The sheath edge is considered to be an absorption surface from which no attracted particles escape.

In the presheath-wake region, and initially for all space, the ion densities are determined by a "neutral ion approximation". This refers to the assumption of straight line trajectories as if following neutral particles. This means that the ion density in this region is calculated taking fully into account ion thermal velocities but ignoring bending of trajectories by electric or magnetic fields. This can be expressed by the following equation:

$$f_i(\vec{x}, \vec{v}) = g(\vec{x}, \vec{\Omega}) \, f_{io}(\vec{v})$$

where $f_i(\vec{x}, \vec{v})$ is the ion distribution function at a point x in space for a velocity $\vec{v}$ and $f_{io}(\vec{v})$ is the unperturbed velocity distribution function for a drifting Maxwellian (the assumed condition at an infinite distance from the vehicle). The function $g(\vec{x}, \vec{\Omega})$ has value zero if a ray starting from $\vec{x}$ going in the direction $\vec{\Omega}$ would strike the vehicle, it has value 1 otherwise. This function takes into account particles which cannot contribute to the local charge density because they run into the vehicle. The ion density is obtained by integration over velocities:

$$n_i(\vec{x}) = \int f(\vec{x}, \vec{v}) dv = \int_\Omega g(\vec{x}, \vec{\Omega}) \int_0^\infty f_{io}(\vec{v}) v^2 dv \, d\vec{\Omega}$$

208

This "neutral ion" approximation to the density is particularly simple to calculate for two reasons. First, the straight line orbits allow trajectories to be "traced" instantly, and second, the orbits, and thus shadowing factors, are independent of particle kinetic energy. For every point in space the basic algorithm finds the perimeter of each object surface in solid angle space and eliminates all orbits within the perimeter from contributing to the local phase space density. While using only discrete directions this technique has been proven fast and reasonably accurate. The major numerical approximations are the discretization of the angles and the interpolation in solid angle space of the surface perimeters. Typically the solid angle space is gridded 36 x 180 and a few extra points are added along each surface edge in order to minimize interpolation errors. Since the potential varies logarithmically with density in the quasineutral region, a factor of 2 error in this density will lead to less than kT/e error in the local potential; thus the approximation is not expected to be a source of any large error. Figure 4 is a contour plot of the neutral ion densities calculated for the shuttle orbiter with Mach velocity, M = 8 in an oxygen plasma. Figure 5 shows the same calculation for our favorite test object, the quasisphere.

A new "experimental" feature for POLAR is an algorithm that provides a "first order" correction for the focusing of ion trajectories by the weak presheath electric fields. This correction is based on a study by Gurevich and Pitaevskii (ref. 10) of the flow of a hypersonic plasma over a semi-infinite wall where they include electric fields in calculating the ion densities in the rarefied region (wake) behind the wall. Neutral gas densities may also be obtained analytically for this same problem. The ratio of the plasma to neutral densities, from the wall problem, is used as a correction factor to the neutral ion approximation densities calculated by POLAR.

In figure 6, we present a comparison of the corrected neutral ion density, calculated by POLAR, with electron density measurements by Murphy et al. (ref. 11). These measurements were made on STS-3 by the PDP Langmuir probe. For STS-3, the estimated range of Mach numbers was 5-8, and the estimated uncertainty in the absolute scale of electron densities was 2-5. POLAR densities were calculated at Mach numbers of 6 and 7 using the shuttle model presented in this paper. A comparison between electron and ion densities is strictly valid only when the plasma is quasineutral and the actual degree to which the wake plasma is quasineutral cannot be determined without a complete analysis; however, the deviations from quasineutrality are probably within the experimental error and numerical uncertainties. The emphasis of this comparison is placed upon the horizontal agreement which demonstrates POLAR's ability to model the wake edge using actual orientation data.

As a calculation proceeds, POLAR locates (by inspection of potentials) those regions where quasineutrality does not hold, defines the sheath to include such regions, and recalculates the ion density there by tracking particles inwards from the sheath. Once these sheath ion densities are available, they replace the neutral-ion densities in the Poisson calculation. This replacement process is currently being implemented in POLAR; the calculations presented here used only the neutral ion densities.

SURFACE CHARGING

The POLAR surface cells are the exposed squares, rectangles, and triangles that border the filled space of each individual volume element containing a piece of the object (sub units of the building blocks used in object definition).

POLAR models the accumulation and transport of charge on the vehicle using a lumped element circuit analogy. In this equivalent circuit, each surface cell and conductor represents a node of the circuit. Surface voltages are updated by implicitly timestepping a differenced approximation to the equation

$$I = C \frac{d}{dt} V(t) - \sigma V(t) \quad ,$$

where I and V are current and voltage vectors with each surface and conductor contributing a component, C is the capacitance matrix, and σ the conductance. The current vector is composed as

$$I = I_i + I_{is} + I_{ae} + I_{aes} + I_{aeb} + I_{ph}$$

where we have the current due to ions, ion impact secondary electrons, auroral electrons, auroral electron secondary and backscatter electrons, and photoelectrons. The auroral electron currents and their secondary and backscatter electron currents are determined each timestep by assuming them to be dependent only on the individual surface voltage, then integrating the model distributions with and without secondary and backscatter yield functions. The ion and ion secondary currents are updated only when the sheath module is called. Note that the ambient electrons are absent from this last equation. Because of their low temperature, they will not contribute significant current to any surface more negative than a few kT/e. When a surface charges positive, it is assumed to be because of their omission and the surface is held near zero until it again shows negative charging behavior. This technique prevents the oscillations that could occur with a combination of large timestep and an extremely voltage sensitive current source.

As mentioned previously, POLAR models the flux, Φ, of the energetic auroral electrons as a combination of power law, hot Maxwellian and Gaussian distributions (ref. 12) given by the following expression:

$$\Phi(K) = AK(K + qV)^{-(\alpha+1)} + F \pi^{-1}(kT)^{-2} K \exp(-(K+qV)/kT)$$

$$+ BK \exp(-(K-K_0)^2/\delta^2)$$

where K is kinetic energy, V is the surface potential, $F = n \cdot \sqrt{kT/2\pi m}$, and A, α, T, B, E_0 and δ are the parameters used to fit spectra. This expression has been fitted to a spectrum observed by the DMSP-F2 satellite (ref. 13),

210

which is shown in figure 7, along with the POLAR fit. This analytic form can be quickly integrated to find the contributed surface current.

At the start of a new calculation, before any sheath calculations have been performed, a vehicle may be started at a uniform voltage, or precharged by using the thermal and ram ion currents to surfaces at zero voltage for the ion currents. For this precharging, the auroral electron currents are calculated and the charging equations solved as described to produce an initial estimate for the surface potentials.

THE CHARGE-STABILIZED POISSON ITERATION

The Poisson equation can be written as

$$-\nabla^2 \phi = \lambda^{-2}(n_i - n_e)$$

(1)

where $\phi = eV/kT$, $\lambda^2 = \epsilon_0 kT/N_0 e^2$, N_0 is the ambient density, and $n_i = N_i/N_0$, $n_e = N_e/N_0$. POLAR solves this equation on its discrete mesh using a finite element method (refs. 14, 15). It is not practical to develop it here, but we will present a few of its pertinent features.

POLAR's finite element formulation assumes a trilinear interpolation function for the potential in spaces so that the influence of each node goes to zero in one mesh unit. This allows for the development of a matrix to approximate $-\nabla^2$ for each element. The finite difference approximation to the equation (1) would be

$$\left(\sum_e \underset{\sim}{w}^e\right) \phi = \lambda^{-2} (\underset{\sim}{n}_e - \underset{\sim}{n}_i) \quad h^3$$

(2)

where h^3 is the volume of element e. However, rather than summing the individual matrices into one large matrix, matrix solvers can be taught to work just as efficiently on the individual element matrices. This produces many advantages. One such advantage is core storage. For a problem with 20,000 grid points, the complete matrix would require 4×10^8 words of storage if no compression methods were used, whereas, there are only a limited number of element types (six so far) requiring less than 1000 words of storage for their matrices. Another advantage is that this method very naturally allows us to solve for potentials with only one slice of elements (two slices of nodes) in core.

The traditional approach to the solution of equation (2) has been an explicit iteration of the form

$$-\nabla^2 \phi^\nu = \lambda^{-2}[n_i(\phi^{\nu-1}) - n_e(\phi^{\nu-1})]$$

(3)

where ν is the iteration index, and the charge density is determined using the potentials of the previous iteration. This method can be shown to be unstable

(ref. 16) when the Debye length, λ, becomes small with respect to other scale lengths of the problem. This can be understood by considering that a smooth potential variation over a distance of, say, 1000 λ, would require a smooth $\nabla^2\phi$ (the "second derivative") which is in turn given everywhere by the charge density. But, maintaining a smooth charge density distribution is difficult when any errors in determining $(n_e - n_i)$ are multiplied by the huge number λ^{-2}. There is one effective remedy to this dilemma (ref. 16) but the process reported here appears to be more efficient in the short Debye length limit. This method involves the combination of two concepts. One uses a partial implicitization of the repelled density (n_e, here) (ref. 17). The other simply reduces the charge density to an acceptable level whenever the first method is inadequate.

Suppose a plasma of ambient density N_0 and temperature T consists of Boltzmann electrons, $N_e(\vec{r}) = N_0 \exp(\phi(\vec{r}))$ and ions of known density $N_i(\vec{r}) = N_0\, n_i(\vec{r})$. The normalized charge density is then given by

$$q(\vec{r},\phi^\nu(\vec{r})) = \lambda^{-2}\,[n_i(\vec{r}) - \exp(\phi^\nu(\vec{r}))] \tag{4}$$

Equation (4) may be linearized about the previous potential iterate

$$q(\phi^\nu) \simeq q(\phi^{\nu-1}) + q'(\phi^{\nu-1}) * (\phi^\nu - \phi^{\nu-1})$$

where $q' = \partial q/\partial\phi$, and the $\vec{r}$ dependence has been dropped for clarity. With this expression we may write the implicit Poisson iteration scheme

$$-\nabla^2\phi^\nu - q'(\phi^{\nu-1}) * \phi^\nu = q(\phi^{\nu-1}) - q'(\phi^{\nu-1}) * \phi^{\nu-1} \tag{5}$$

Though it is not immediately obvious, the implicit character of (5) makes it more stable than scheme (3). This can be understood by realizing that in equation (3) the electron density was treated as an independent variable, whereas in (5) the electron density is determined simultaneously with the potential, both being consistent with the ion density.

The finite element approximation to (5) produces the matrix equation

$$\sum_e (\underset{\sim}{W}^{(e)} - \underset{\sim}{S}'^{(e)}\, \underset{\sim}{V}^{(e)}) * \underset{\sim}{\phi}^\nu = \underset{\sim}{S} - \underset{\sim}{S}' * \underset{\sim}{\phi}^{\nu-1} \tag{6}$$

where S is derived from q by the following analysis:

For small h/λ, S is simply the total charge associated with each node, $Q = q\, h^3$. If the elemental volume becomes large compared to λ, then numerical noise and features like a sheath edge which may span only a few λ, becomes incorrectly amplified when the q determined at a point becomes multiplied by all of h^3. When it is not possible to reduce the zone size, stability can be preserved by replacing Q (and Q') with a reduced value S (S')

which is calculated to be the maximum allowable charge for the element. Because of the artificial amplification argument, S is often the more realistic total for an element. Before deriving S, we define the barometric potential $\phi_b = \ln(n_i)$ which is the potential for which $Q = 0$ and note that it is important that $S \rightarrow Q$ as $\phi \rightarrow \phi_b$ if quasineutral regions are to be modeled correctly. To determine S, consider a capacitor with potential difference $(\phi_b - \phi)$, area h^2, and a separation of h. The charge q_c on this capacitor is given by

$$q_c = C\Delta V = \frac{\epsilon_o h^2}{he} (\phi_b - \phi)kT$$

In the units of our previous Q, q_c becomes

$$Q_M = \alpha h(\phi_b - \phi)$$

which is the maximum allowable charge per element, with the parameter α, adjusted to insure that Q_M is maximized. Thus at each node, we choose for the charge

$$|S| = \min.(|Q_M|, |Q|)$$

with

$$S' = \begin{cases} -\alpha h & \text{for } S = Q_M \\ -h^3\lambda^{-2} \exp\phi & \text{for } S = Q \end{cases}$$

The effect of this algorithm is this: If a problem has been specified where a boundary potential would be screened in less than a zone or two (the limit of any code's resolution), sufficient sheath charge will be redistributed so as to allow the potential to be screened over the minimum number of zones that are consistent with stability. When this occurs it is necessary to have a modified criteria for locating the sheath "edge". Our choice is to place the edge at $\phi_m = \ln(\alpha\lambda^2/h^2)$ (when $\phi_m > kT/e$) which is the potential at which $Q'_n = Q'$. This is the potential contour that marks the region where the most drastic charge reduction occurs.

SHEATH PARTICLE TRACKING

Internal to the sheath boundary, strong electric fields will cause significant bending of ion trajectories and focusing of currents. POLAR models these effects by tracking "particles" inward from the sheath edge to the object surface. This tracking provides both the distribution of surface currents, i.e. currents to surfaces, and the ion density within the sheath. Prior to performing this calculation, we must know the suitable sheath location and the currents from the plasma to the sheath.

The sheath edge can be thought of as an absorption surface where for the attracted species (ions, here) there is only flow in, none out. If this surface were the same for all ion energies, and there was no presheath focusing, we would find that in a non-flowing plasma, the density just outside the sheath edge to be $n_{is} = 1/2\ n_0$. We can next invoke quasineutrality with Boltzmann electrons

$$n_e = n_0\ e^{\phi_s} = n_{is} = n_0/2$$

and find for a sheath edge potential $\phi_s = -\ell n2 = -0.69$. In their treatment of space charge limited probes, Parrot et al. (ref. 18) indicate that in a non-flowing Maxwellian plasma, the sheath edge potential ϕ_s of a spherical probe asymptotically approaches the value -0.49 (-0.86 for a cylinder) as the ratio of surface potential to plasma temperature becomes infinite. For a probe in a flowing plasma, the most distended absorption surface is likely not to be an equipotential. In the ram direction, we would expect $\phi_s \rightarrow 0$, whereas in the wake direction we can conjecture that the sheath edge potential would lie in the range $1/2 > \phi_s > M^2/2$, where M is the Mach number. The degree of importance placed upon accurately locating the sheath edge must consider the resulting effects on the primary issue, surface charging. POLAR currently uses an equipotential chosen as described in the previous section. This numerically defined sheath boundary typically lies in the quasineutral region.

Ions dropped inwards from the sheath boundary are assigned currents according to the calculated presheath current to their points of origin. For the case of a non-flowing plasma, Parrot et al. (ref. 18) have determined the presheath current enhancement to be $J/J_0 = 1.45$ for both spherical and cylindrical cases, where $J_0 = N_0(kT/2\pi m)^{1/2}$ is the ambient thermal current. To find this enhancement for an arbitrarily specified boundary in a flowing plasma, we make the approximation that in the presheath region currents may be calculated from orbit limited theory, i.e., an outwardly directed hemisphere of trajectories will all connect to infinity if the total trajectory energy is greater than zero. For the case of a $1/r$ potential distribution in a non-flowing Maxwellian plasma (ref. 19), this approximation would lead to the well-known Langmuir formula

$$J = J_0\ (1 - \phi_s) = 1.49, \text{ for } \phi_s = -0.49$$

This can be compared to the 1.45 given by Parrot et al. (ref. 18). For our flowing plasma, we assume a $1/r^2$ potential (the most rapidly diminishing for which all energetically allowed trajectories may escape) (ref. 20), and the flowing distribution at infinity

$$f_{i\infty} = N_0(2\pi)^{-3/2} \exp\left[-\frac{1}{2}\ (\vec{V}-\vec{M})^2\right]$$

Sheath surface current densities are determined by numerically calculating the first velocity moment of the sheath surface distribution function. Results

are presented in figure 8 for three sheath surface potentials. The curves for higher potential in figure 8 are consistent with the orbit limited approximation in the wake-ward direction only. Elsewhere the higher potentials would be screened more rapidly than $1/r^2$.

Return now to the question of sheath boundary placement. The results of figure 8 indicate that the current density enhancement factors are not tremendously sensitive to the sheath boundary potentials for the ram-ward angles. For wake-ward angles, there is a much greater enhancement sensitivity but this may not carry over into a surface charging sensitivity. A lower potential sheath boundary will tend to extend ellipsoidally in the wake direction producing increased sheath surface area. Focusing within the sheath/wake area will collect these lower sheath currents and reduce the sensitivity to sheath boundary placement. Also, all of these wake/sheath currents are small, and may ultimately be negligible when compared to other positive current sources such as the contribution from secondary electrons and the hydrogen component, for which the Mach speed will be a factor of 4 less than for oxygen. The paper by Parks et al. in these same proceedings investigates the effects of a hydrogen component.

In each spatial element, the sheath edge is contoured by triangular plates. From each, two or more (typically four) particles are started. Before these particles are assigned currents, a test particle is ejected outward from each plate across a few elements to probe for objects or potential barriers that would shield presheath currents from that plate. If such obstacles are formed, the particles from that plate are deleted.

Once all particles and currents have been assigned, particles are advanced along their trajectories by a "pusher". This pusher sweeps back and forth along the Z axis, operating on successive single slices of elements (two slices of nodal potentials). Within each slice, trajectories advance in the X and Y directions until they reach the present Z or Z+1 slice boundaries, X, Y boundaries or the vehicle surface. If the pusher is sweeping in the +Z direction, particles exiting at Z+1 are continued in the next push, whereas particles exiting at Z (moving in the -Z direction) are stored on disk and picked up on the return pass of the pusher. The pusher continues sweeping until all trajectories have been concluded.

RESULTS

Two model calculations are presented, the quasisphere and the shuttle. For both problems, the plasma is an O^+ plasma with $kT = 0.1$ eV, $N = 10^4$ cm^{-3} and $\lambda = 2.3$ cm. Both models have the objects moving at an ion Mach speed of 8 (~8 km/sec). Neutral ion density contour plots for these objects have been presented in figures 4 and 5. All of the contour plots are 2-D cuts through the 3-D arrays of potentials or densities. In the quasisphere (Q-S) plots, the cuts go through the center of the object and its wake. For the shuttle, the longitudinal cuts (showing a side profile of the orbiter) run just to the side of center and through one of the engines.

In these calculations, the Q-S is modeled as a grounded conductor covered with 0.1 mm thick kapton and a "quasiradius" of 2.5 m. At $t = 0$, the auroral spectrum of figure 7 is switched on, with all surfaces at zero potential. The Q-S is allowed to charge for a total of 7.8 seconds in 13 intervals

of 0.6 sec each. Ambient electron spacecharge factors and auroral electron surface currents are calculated at each step. All secondary electrons are assumed to escape. Ion surface currents are determined from sheath particle tracking at the 0.6, 2.4, 4.8 and 7.2 sec intervals, while the 0-0.6 sec interval uses the precharge estimates of ion currents. Figure 9 shows a potential contour plot with linearly spaced contours at 2.4 sec, where the maximum surface potential is -130 volts on the wake side of the Q-S. Figur 10 is a contour plot of the same potentials using logarithmically spaced cr. tours, where the sheath contour is chosen to be -0.6 volts and is indicated by the X's. A subset of the sheath ion trajectories are also shown. Figure 11 shows linear potential contours for the Q-S at 4.8 seconds with the new sheath location (-0.6 volts) indicated again by X's; the maximum surface potential is -252 volts. The end point of the calculation is shown in figure 12 at 7.8 seconds where a rough equilibrium has been established and the maximum surface voltage is -447 volts. The apparent discharging of the side surfaces at 7.8 seconds when compared with the Q-S at 4.8 seconds is a plotting illusion due to the same number of contours being spread over a large potential difference. The long charging times reported here are not realistic and are due to the combination of grounded conductor and thin dielectric which produces a high capacitance to ground. This fixed ground has been retained as a developmental convenience and will be allowed to float in the future.

A preliminary model of shuttle orbiter charging is presented in figures 4, 13, 14, and 15. The materials specified for this model are not realistic, and again, the ground was not allowed to float. Starting with the ion densities shown in figure 4, the orbiter is exposed to the same plasma and aurora as was the Q-S with a mesh spacing of 1.16 m/grid unit. The shuttle is allowed to charge for only 3 seconds in three steps. Potential contours at the 3 second point are presented in figure 13 for the same cut as figure 5. The maximum surface potential is -101 volts. The lowest contour is at -20 volts so it is not possible to see lower space potentials in the wake, but one can observe the compression of contours on the underside compared to those in the cargo bay. Figure 14 is a cut through the ion density data at Z = 17 (see figure 13). In figures 14 and 15, the complete projected silhouette is outlined whereas only a portion of the cargo bay floor, wall and doors actually lie in this cut. Since the plasma is flowing predominantly along the length of the orbiter, the ion density wake shown in figure 14 is due to portions of the orbiter upstream of the cut. Figure 15 shows potential contours in the cut at Z = 17, where significant charging can be observed on the outside of the bay doors which lie in the wake of the wings, but not on the inside which was a grounded conductor.

The shuttle model employed 41,175 grid points, but due to POLAR's disk data management and segmented construction, only about 70,000 words of core memory were required. On our UNIVAC 1100/80, the shuttle model calculation required about 3 hours of CPU time.

CONCLUSIONS

The results of these POLAR calculations are quite preliminary and are presented primarily to demonstrate the capabilities of the code. However, we are quite pleased with the close resemblance of the quasisphere model to the DMSP charging events reported in these same proceedings by Burke and Hardy. Perhaps the most significant result of these calculations is that POLAR's

design criteria are proving to be realizable, and although more development will be required we anticipate that POLAR will become a useful scientific and engineering tool.

ACKNOWLEDGMENTS

REFERENCES

1. Katz, I. and D. E. Parks: Space Shuttle Orbiter Charging. J. Spacecraft and Rockets, 20, 1983, pp. 22-25.

2. Parker, L. W.: Plasmasheath-Photosheath Theory for Large High-Voltage Space Structures. Progress in Astronautics and Aeronautics, Space Systems and Their Interactions with Earth's Space Environment, 71, AIAA, New York, 1980, pp. 477-522.

3. McCoy, J. E., A. Konradi and O. K. Garriott: Current Leakage for Low Altitude Satellite. Progress in Astronautics and Aeronautics, Space Systems and Their Interactions with Earth's Space Environment, 71, AIAA, New York, 1980, pp. 477-522.

4. Cohen, H. A. et al.: P78-2 Satellite and Payload Responses to Electron Beam Operations on March 30, 1979. USAF/NASA Spacecraft Charging Technology Conference III, NASA CP-2182, AFGL-TR-81-0270, 1980, p. 509.

5. Olsen, R. C. and C. K. Purvis: Observations of Charging Dynamics. J. Geophys. Res., 88, 1983, pp. 5657.

6. Raitt, W. J., P. M. Banks, P. R. Williamson, K. D. Baker, T. Obayaski and J. L. Burch: Early Experiments in Charged Particle Beams From the Space Shuttle. Presented at AIAA 20th Aerospace Sciences Meeting, Orlando, FL, 1982.

7. Linson, L. M.: Current-Voltage Characteristics of an Electron-Emitting Satellite in the Ionosphere. J. Geophys. Res., 74, 1969, p. 2368.

8. Winkler, J. R.: The Application of Artificial Electron Beams to Magnetospheric Research. Rev. Geophys. and Space Physics, 18, 1980, pp. 659-682.

9. Katz, I., M. J. Mandell, G. W. Schnuelle, J. J. Cassidy, P. G. Steen and J. C. Roche: The Capabilities of the NASA Charging Analyzer Program. Spacecraft Charging Technology-1978, NASA CP-2071, AFGL-TR-79-0082, 1979, pp. 123-143.

10. Gurevich, A. W., L. W. Pariiskaya and L. P. Pitaevskii: Self-similar Motion of Rarefied Plasma. Soviet Physics, JETP, 22, 1966.

11. Murphy, G. B., S. D. Shawhan, L. A. Frank, J. M. Grebowsky, D. L. Reasoner, N. Stone, N. D'Angelo and D. A. Gurnett: Interaction of the Space Shuttle Orbiter With the Ionospheric Plasma. Presented at 17th ESLAB Symposium, Spacecraft-Plasma Interactions and Their Influence on Field and Particle Measurements, Noordwijk, Netherlands, 1983.

12. Fontheim, E. G., K. Stasiewicz, M. O. Chandler, R. S. B. Ong, E. Gombosi and R. A. Hoffman: Statistical Study of Precipitating Electrons. J. Geophys. Res., 87, A5, 1982.

13. Hardy, D. A.: The Worst Case Charging Environment. Proceedings of Air Force Geophysics Laboratory Workshop on Natural Charging of Large Space Structures in Near Earth Polar Orbit: 14- 15 September 1982, AFGL-TR-83-0046, January 1983.

14. Stannard, P. R., M. J. Mandell and I. Katz: NASCAP Programmers Reference Manual. S-CUBED Report SSS-R-82-5443, March 1982.

15. Strang, G. and G. J. Fix: An Analysis of the Finite Element Method. Prentice-Hall, George Forsythe, ed., 1973.

16. Parker, L. W. and E. C. Sullivan: NASA Report No. NASA TN D-7409, 1974.

17. Parker, L. W.: Calculation of Sheath and Wake Structure About a Pillbox-Shaped Spacecraft in a Flowing Plasma. Proceedings of the Spacecraft Charging Technology Conference, AFGL-TR-77-0051, NASA TMX-73537, 1977.

18. Parrot, M. J. M., L. R. O. Storey, L. W. Parker and J. G. Laframboise: Theory of Cylindrical and Spherical Langmuir Probes in the Limit of Vanishing Debye Number. Phys. Fluids, 25, 1982.

19. Laframboise, J. G. and L. W. Parker: Probe Design for Orbit-Limited Current Collection. Phys. Fluids, 16, 5, pp. 629, 1973.

20. Laframboise, J. G.: Theory of Spherical and Cylindrical Langmuir Probes in a Collisionless, Maxwellian Plasma at Rest. UTIAS Report 100, 1966.

21. Al'pert, Y. L., A. V. Gurevidh and L. P. Pitaevskii: Space Physics with Artificial Satellites. Consultants Bureau, New York, 1965.

TABLE 1. – POLAR/IONOSPHERIC PARAMETERS

Orbit Altitude	150–350 km

Ambient Plasma
- Temperature (eV) — 0.1–0.3
- Ion Density(cm^{-3}) — 10^4–10^6
- Ion Species — O^+, N^+, He^+, H^+
- Neutral Density (cm^{-3}) — 10^8–10^{11}

Ambient Electron Acoustic Speed — $V_{ae} = \sqrt{kT/m} = 133$ km/sec

Ambient O^+ Acoustic Speed — $V_{ao} = 1$ km/sec

Satellite Velocity — 8 km/sec, $\vec{M} = \vec{V}/V_{ao} = 8$

Auroral Electrons
- Energies — $\approx 10^2$–10^5 eV
- Fluxes — $< 10^9/cm^2 \cdot sec \cdot str \cdot KeV$
- Integrated Currents — $< 100\ \mu A/m^2$

Magnetic Parameters

Magnetic Field Strength — 5×10^{-5} Tesla (0.5 Gauss)

Particle	Gyroradius	Gyroperiod
Ambient Electrons	(0.1 eV) 2 cm	
Secondary Electrons	(3 eV) 13 cm	7×10^{-7} sec
Auroral Electrons	(10 KeV) 4 m	
Ambient Ions (O^+, 0.1 eV)	3 m	2×10^{-2} sec
(H^+, 0.1 eV)	0.2 m	1.3×10^{-3} sec

Cycloid Spacing Observed At 8 km/sec
- Electrons — 0.6 cm
- H^+ — 10 m
- O^+ — 160 m

Characteristic Lengths

Ambient Debye Length	$\lambda_D \leq 1$ cm	
Shuttle Orbiter	$L = 37$ m	

	1 kV	5 kV
Sheath Thickness For Potentials		
Around 3 m Radius Sphere [+] [**]	6.9 m	11.6 m
Planar Child-Langmuir [+]	9.32 m	31.2 m

[+] Calculated for $\lambda_D = 0.74$ cm, $kT = 0.1$ eV
[**] From Figure 72, Al'pert et al. (ref. 21)
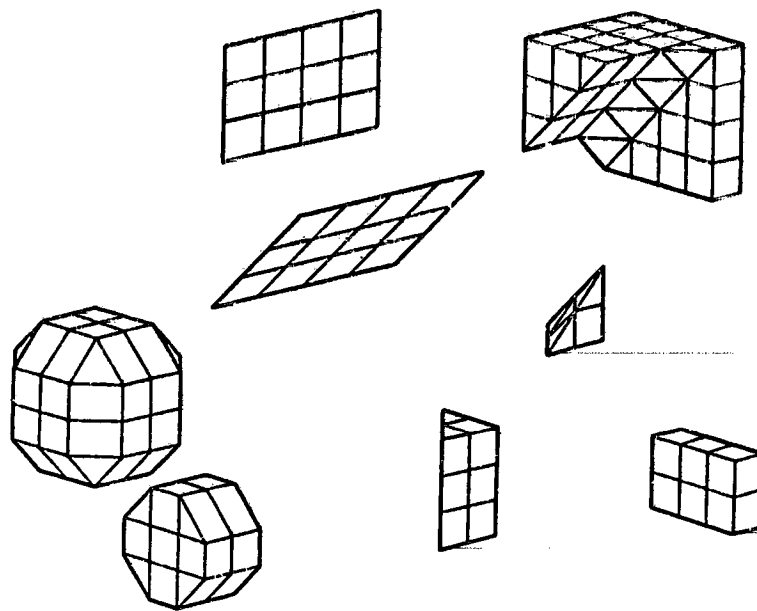
Figure 1. The eight building block types are shown here. From right to left and top to bottom: flat plate, FIL111 smoothing a corner, slanted plate, tetrahedron, quasisphere, wedge, rectangular parallelepided, and octagon right cylinder.
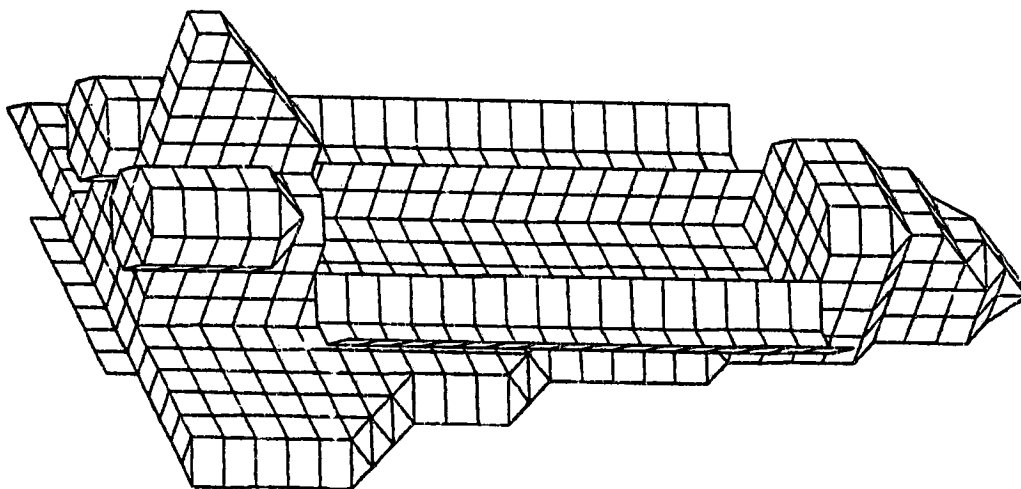
Figure 2. Perspective plot of the POLAR shuttle model used for these calculations, showing individual surface cells.
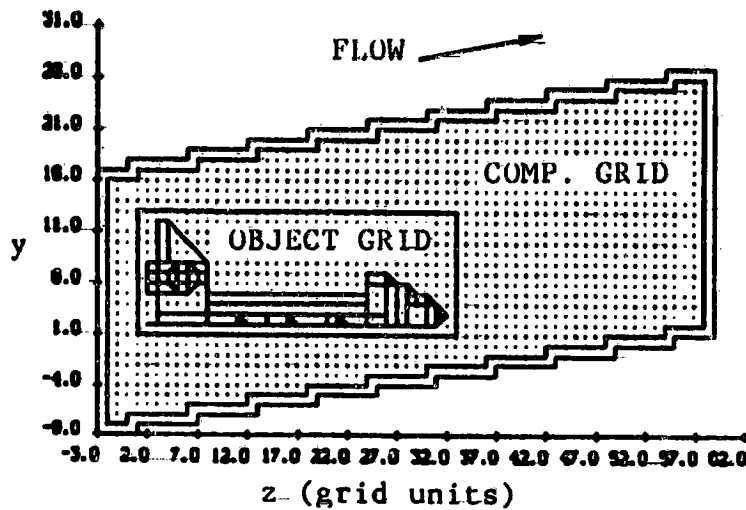
Figure 3. Two-dimensional cross-section of POLAR's computational and object grids. The combination of orthogonal transformations of the object and object grid with staggering in the X·Y node slices allows for any orientation of object and plasma flow.
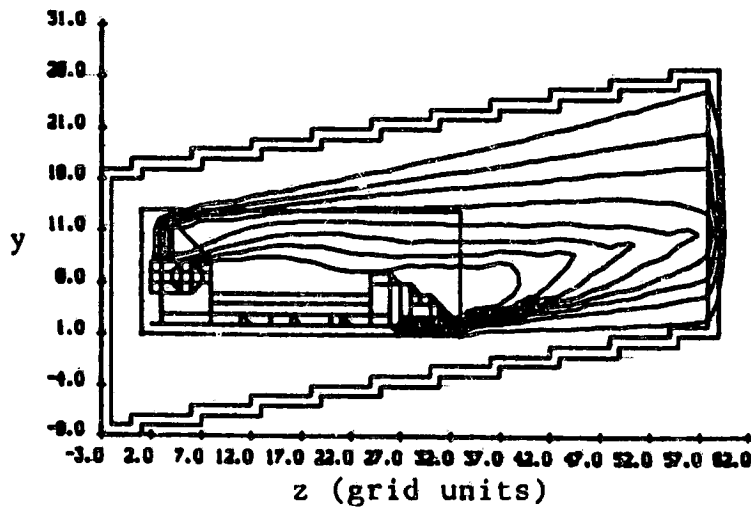
Figure 4. Two-dimensional cross-section of normalized neutral ion densities, for a slice one unit from center, running through an engine. One mesh unit = 1.16 m, ion Mach speed = 8, contour interval = 0.11, $N_0 = 10^4$ cm^{-3}, kT = 0.1 eV.
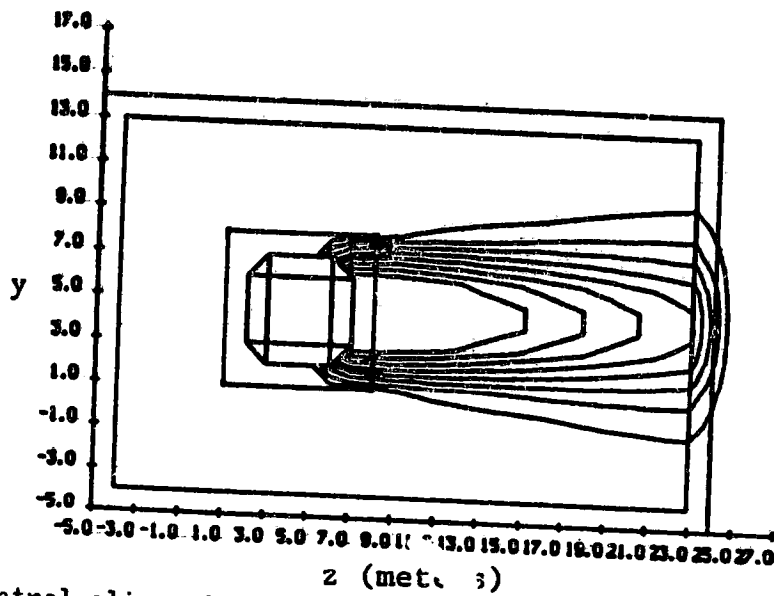
Figure 5. A central slice of ion density contours for a quasisphere. One
mesh unit = 1.0 m, ion Mach speed = 8, kT = 0.1 eV, contour inter-
val = 0.11.
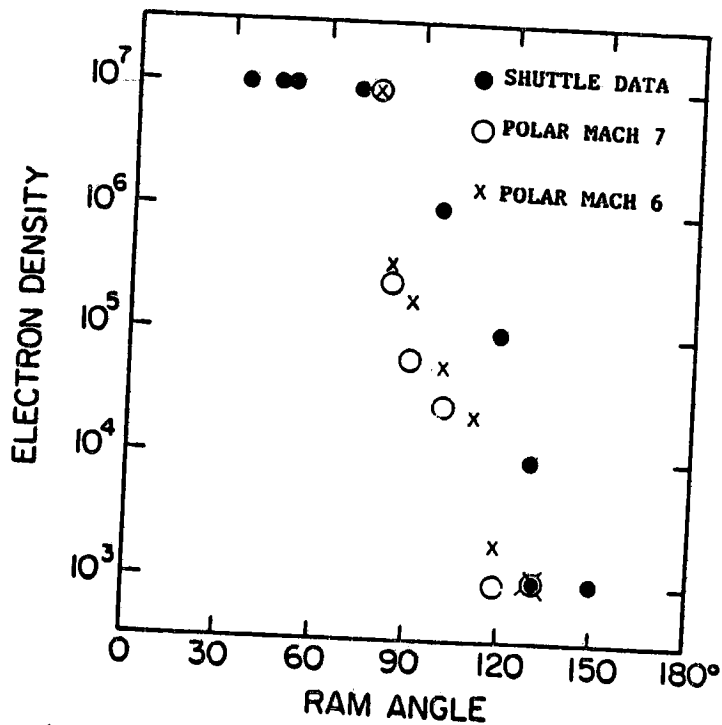
Figure 6. POLAR code calculation of shuttle cargo bay plasma densities
compared with measurements made by Murphy et al. (ref. 11).

222

DIFFERENTIAL ELECTRON FLUX
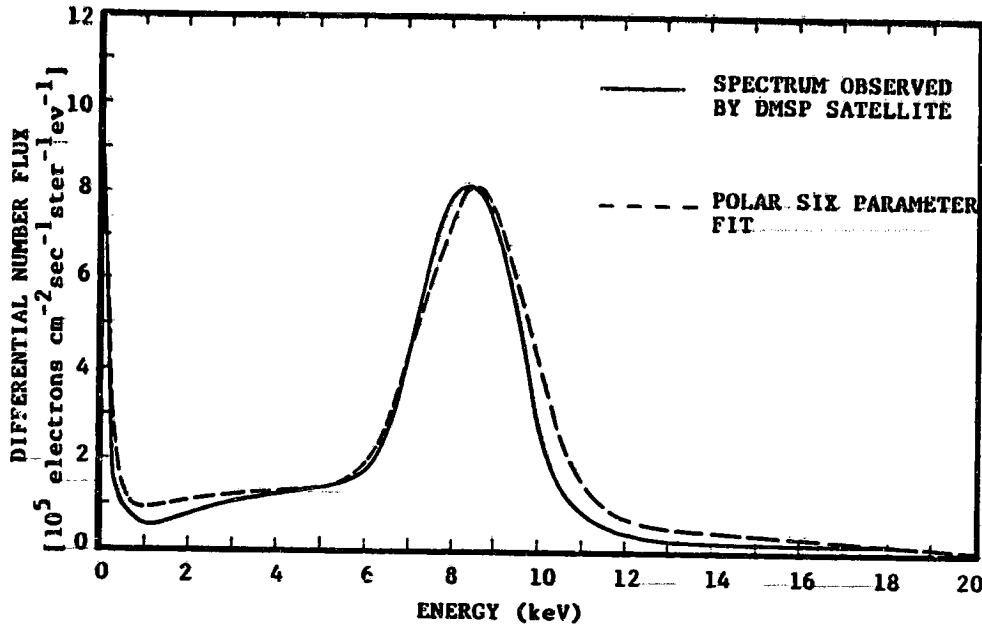
Figure 7. Fit and comparison of POLAR's analytic spectral form to an energetic electron event observed on DMSP-F2 (ref. 13). Assuming isotropy the total current carried by this spectra was 14 $\mu A/m^2$.

J/n_o V_{th}	$\cos(\theta)$	PHI
7×10^{-17}	-1.0	0
5×10^{-8}	-1.0	10.0
7×10^{-4}	-1.0	30.0
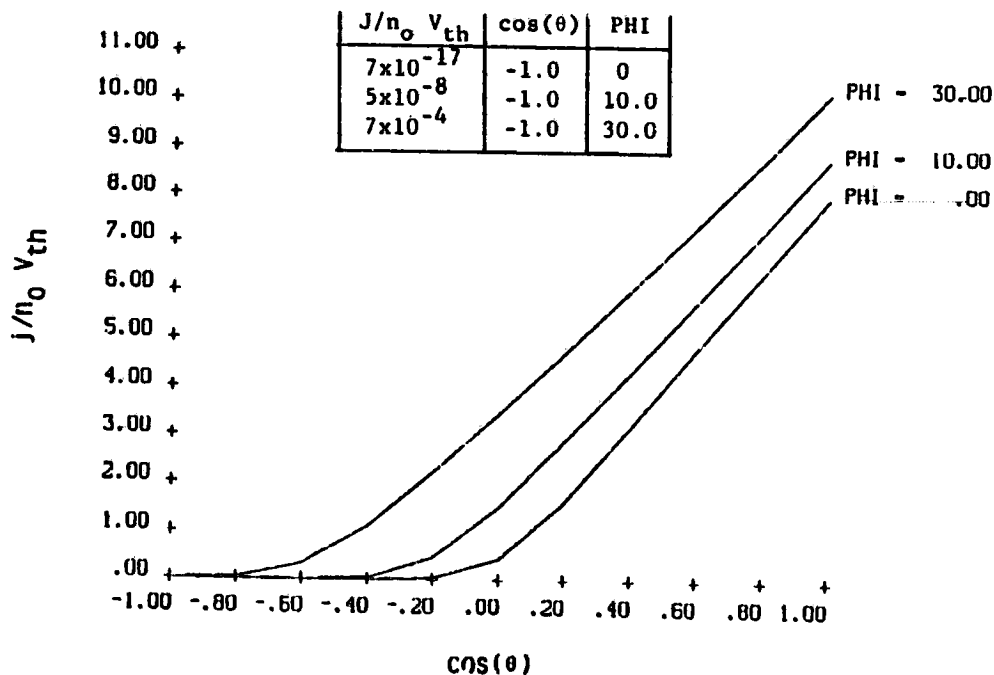
Figure 8. Current density to a sphere of potential PHI = eV/kT in a Mach 8 plasma using orbit limited theory, $\cos(\theta)$ = 1.0 for ram direction, $\cos(\theta)$ = -1.0 for wake direction.

223
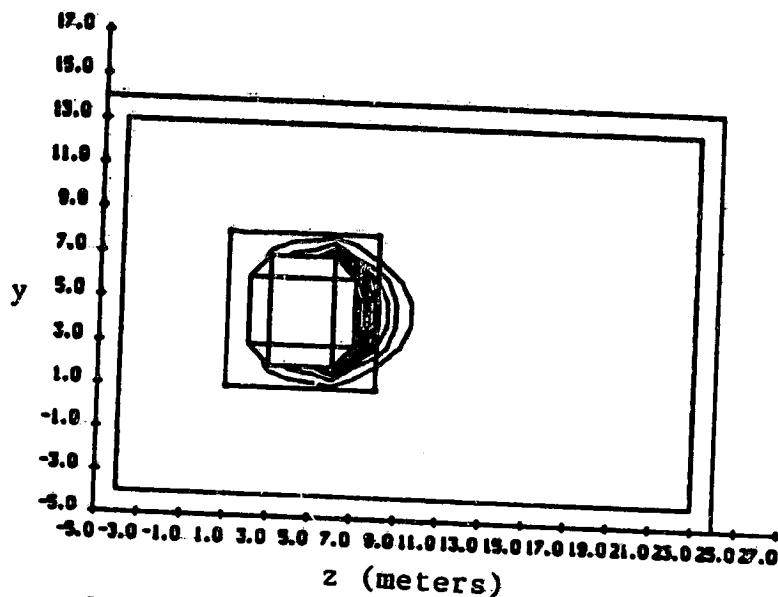
Figure 9. Contour plot of potentials for the quasisphere in the same cross-section as figure 5 after 2.4 seconds of charging. Contour intervals are 14.5 volts, and the maximum surface potential is -130.0 volts. The ambient plasma density is 10^4/cc, kT = 0.1 eV, and λ_D = 2.3 cm.
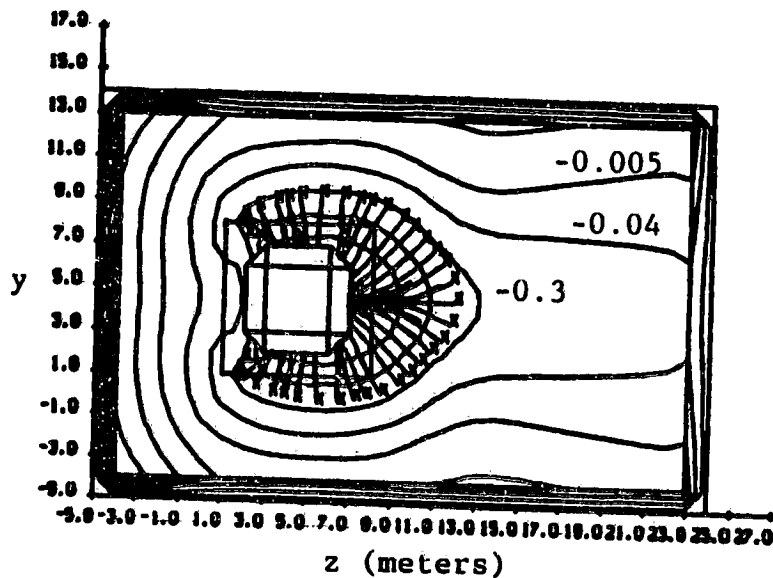

Figure 10. The same potentials and cross-section as figure 9, but with logarithmic contours. The contour interval is $\Delta\log(-V)$ = 0.87, labeled contours are in volts. The lower left tip of the x's mark the sheath location (-0.6 v), where a subset of trajectories illustrate the sheath ion tracking.
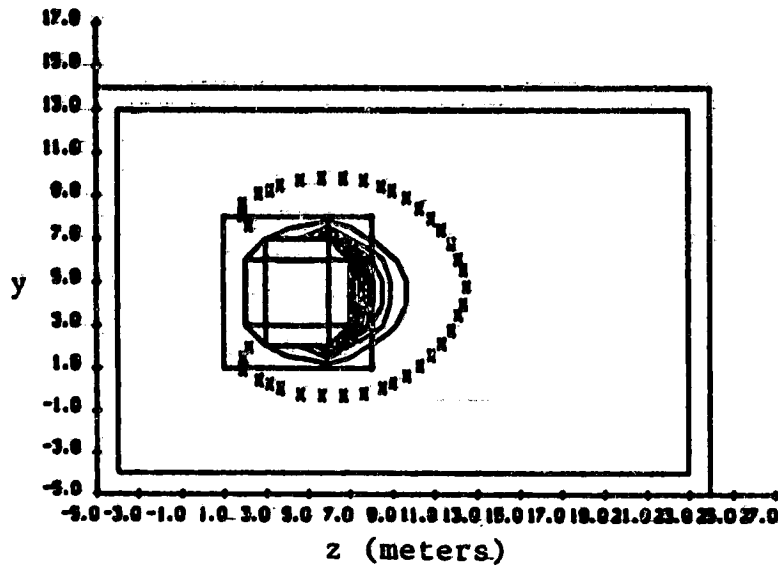
Figure 11. Quasisphere potential contours after 4.8 secs of charging. The maximum surface potential is −252 volts, and the contour interval is 28 volts. X's again mark the −0.6 volt sheath contour.

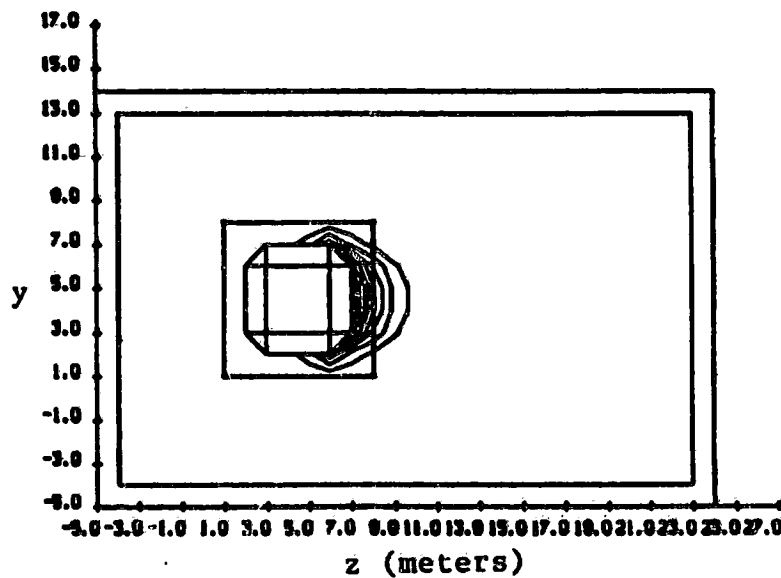Figure 12. Quasisphere potential contours after 7.8 secs of charging, where some surfaces have reached equilibrium. The maximum surface potential is −447 volts and the contour interval is −49.7 volts.
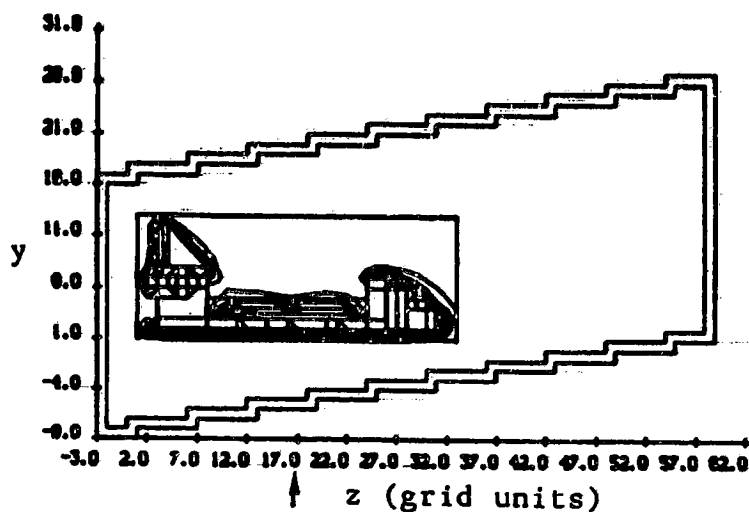
225

Figure 13. Contour plot of potentials about the shuttle orbiter in the same cross-section as figure 4. The maximum surface potential in this cross-section is -101 volts, and the contour interval is 20 volts. The arrow at $Z = 17$ indicates the location of cross-section shown in figures 14 and 15.
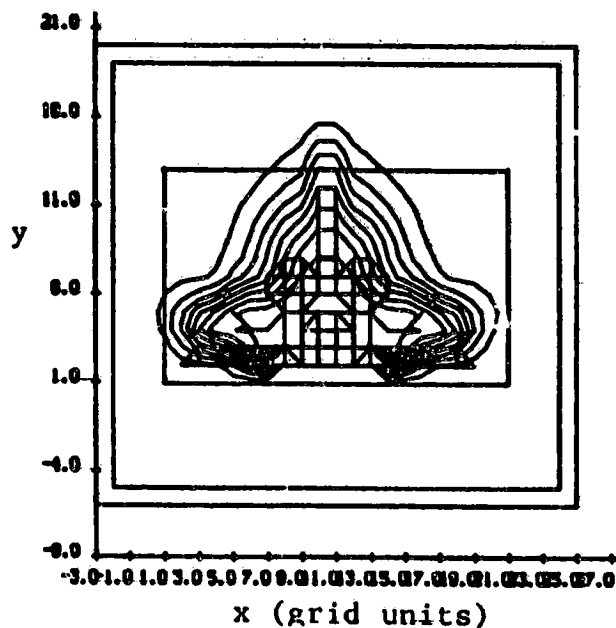

Figure 14. Ion density contour cross-section at $Z = 17$ (see figure 13). The full projected sillouhette of the orbiter is shown, although only cargo bay walls, doors, and floor lie in this slice. Ion densities range from 8×10^{-7} to 1.0 in intervals of 0.11.
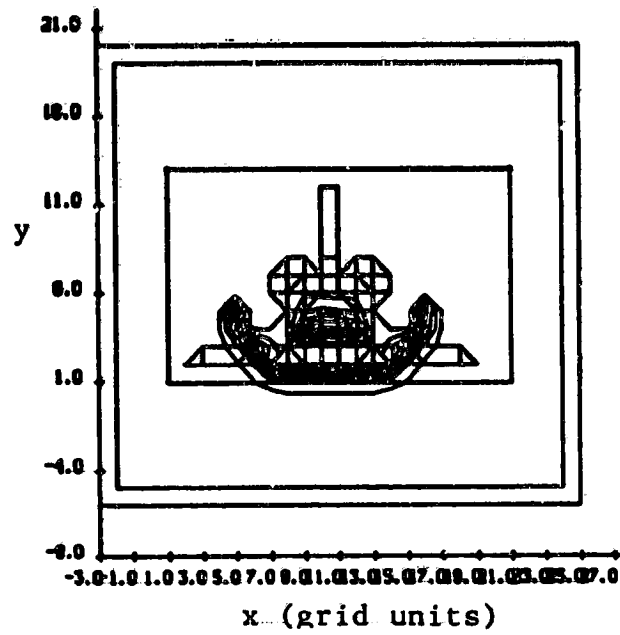
226

Figure 15. Shuttle potential contours in the cross-section of figure 14. The maximum surface potential in this slice is -101 volts and the contour level is 11 volts.